Simultaneous Distributed Sensing on Multiple MgO-Doped High Scattering Fibers by Means of Scattering-Level Multiplexing

Aidana Beisenova, Aizhan Issatayeva, Sanzhar Korganbayev, Carlo Molardi, Wilfried Blanc, Daniele Tosi

Simultaneous Distributed Sensing on Multiple MgO-Doped High Scattering Fibers by Means of Scattering-Level Multiplexing

Aidana Beisenova, Aizhan Issatayeva, Sanzhar Korganbayev, Carlo Molardi, Wilfried Blanc, and Daniele Tosi

***Abstract*—We introduce a novel multiplexing technique applied to optical fiber distributed sensors, based on optical backscatter reflectometry (OBR) and high-scattering MgO-doped fibers. In this paper, we demonstrate the possibility of simultaneously detecting multiple fiber with a single scan using an OBR distributed sensor, and successfully discriminating each sensing region (with ∼1 mm spatial resolution). The sensing element is a high-scattering fiber with MgO-based nanoparticles doping in the core, that emits a scattering signal more than 40 dB larger than a standard fiber, while having similar temperature and strain sensitivity. Multiplexing occurs as the scattered light from a sensing fiber overshadows the amount of scattering occurring in all the other channels. The setup has been validated for temperature sensing and implemented in an epidural catheter with multiple fibers fixed to the outer walls for strain sensing. The proposed solution goes beyond the multiplexing methods which exploit 1 × N switches, as the multiplexing is simultaneous and not rearranged in different time slots.**

***Index Terms*—High scattering fiber, microstructured fibers, optical backscatter reflectometry, optical fiber sensors, spatial multiplexing.**

I. Introduction

OPTICAL fiber sensors (OFS) have been consolidated as a technology capable of high-performance sensing, and have found significant applications [1]. OFS have been particularly appreciated for their small size and lightweight form factor, intrinsic safety, long-range detection, and immunity to electromagnetic interference [2]. Recently, there has been a significant progress on OFS technology for medical applications, since optical fibers are inherently biocompatible, in accordance to ISO 10993 standard [3], they can support minimally invasive treatments [4], and are MRI-compatible [5].

Recent OFS systems have sustained a generational increment of capacity with respect to the original grating-based sensors and interferometers [1], for the capability of obtaining multiple sensing points on the same fiber and/or split the sensing system onto multiple fibers [6], [7]. These features have substantially enlarged the capability of OFS-based sensing systems, stacking hundreds of sensors in a compact shape [8], [9], and with the possibility of precisely control the geometry of the sensors [10], up to the measurement of bending shape and temperature patterns [11], [12].

The possibility to resolve physical parameters (temperature, strain, pressure) at the millimeter-scale has been analyzed by Tosi *et al.* [13], and is a pivotal key enabling technology in medicine for endoscopic [8] and percutaneous measurements [14], having significant impact in several applications. Among others, resolving in-line temperature at the millimeter scale is essential for real-time monitoring of cancer thermo-therapies, determining the effect of thermal doses into solid tumors [13]; robotic surgical systems make use of bending sensors to detect the shape of micro-manipulators in minimally invasive surgery [10], such as vitreoretinal surgery [15]; sensors mounted inside [16], or on the external walls of needles [17], detect the position of endoscopic or laparoscopic catheters. All these systems have in common the requirement for spatially resolved physical sensing below the centimeter scale of spatial resolution, with the possibility of enabling multi-fiber sensing.

Multiplexing is one of the keys to access multi-sensing systems [18], [19]. Fiber Bragg Grating (FBG) sensors systems make use of time- and wavelength-division multiplexing (WDM) for in-line [8] or matrix-like [14] sensing arrays. WDM can apply to FBGs since each grating has a resonant spectrum that covers a narrow bandwidth, allowing an efficient use of the spectral window of infrared spectrometers and FBG interrogators. On the other side, FBGs are strongly limited in spatial resolution, both by technological limitations to inscribe adjacent FBGs in the fiber, and by the need to have a sufficient reflectivity. FBG arrays fabricated with drawing-tower method typically achieve a spatial resolution of ∼1 cm [20], [13],

insufficient to sustain the aforementioned applications. Recent advances in spatial division multiplexing (SDM), using multi-core fibers, have slightly changed the scenario [21]; most remarkably, Gasulla *et al.* presented a multi-core FBG architecture that couples SDM and WDM with a microwave photonics interrogator [22].

Distributed sensing can achieve a much narrower spatial resolution, approaching the millimeter scale [23], whereas optical frequency domain reflectometry (OFDR) can achieve resolution down to the $\sim$0.1 mm level [24]. From the application perspective, the most important implementation of OFDR is the optical backscatter reflectometer (OBR), conceptualized in [25], [26] and recently industrialized [27]: in this case, the photodetector has enough sensitivity to detect the multiple reflections due to Rayleigh scattering in the fiber, thus there is no need for a cascaded reflective element in the fiber such as a weak all-grating fiber or cascaded reflector [28], but a single-mode (SM) standard fiber itself can serve as a sensor.

When addressing advanced applications, the OBR is inherently limited by the fact that only one fiber can be interrogated. It is possible to connect a $1 \times$ N switch to select multiple output fibers, but in this case the system is slow $(<< 1$ Hz$)$ since each channel has to be triggered and referenced separately [26], [27]. In order to address the aforementioned applications, there is an inherent need for an OBR system that can couple the sub-mm spatial resolution with the possibility of simultaneously operating with multiple fibers. Such system would be able to provide a planar temperature measurement, similar to a magnetic resonance imaging but with a low-cost fiber [29] or mount multiple fibers on a catheter wall to measure multi-dimensional bending [10].

In this work, we introduce a new multiplexing paradigm that is able to configure an OBR distributed sensing system for multi-fiber operation, with a single scan. The key element of the setup is a fiber doped with MgO-based nanoparticles in the core, that results in a scattering much larger than a single-mode fiber. This scattering can show an increment that can be around 40 dB or larger. By appropriate selecting some delay line elements, it is possible to multiplex a plurality of fiber; the underlying principle is that the scattering component from the MgO-doped fiber is much greater than the sum of all the scattering from the other fibers, thus the spectrum observed by the OBR can be unambiguously associated to each sensing region. This work significantly extends the results from Parent *et al.* [30], that used high-scattering fibers for improving the strain accuracy. We demonstrate that, limiting the sensing region to few tens of centimeters for each fiber, it is possible to arrange a simultaneous distributed detection of multiple fibers (both for temperature and strain sensing), without the need for additional in-fiber device, thus proposing a scattering-level multiplexing concept. The concept is demonstrated in a temperature detection setup and is implemented for strain detection using 3 fibers mounted externally to an epidural needle.

The manuscript is arranged as follows: the first section is dedicated to the description (fabrication and properties) of the nanoparticles doped fiber (NP fiber) which is the key player in the new paradigm of distributed sensing multiplexing presented here.

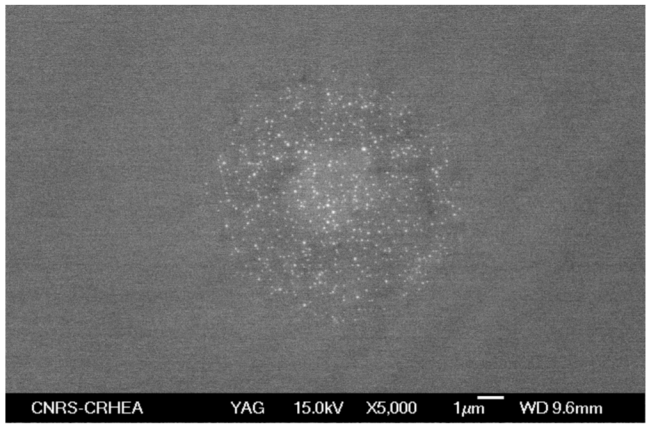

Fig. 1. SEM image of the MgO-based nanoparticles doped fiber. This fiber presents a high level of backscattering which is exploited for obtaining the spatial multiplexing discrimination.

In the second section the working principles of the multiplexing paradigm for OBR distributed sensing is explained and quantified. The third section is dedicated to the proof of concept of the new method, obtained by multiplexing 3 fibers and experimentally sensing temperature and strain. The last section is to draw some conclusions.

II. Nanoparticles Doped Fiber

The key idea for effectively discriminate a parallel optical circuit made by N spatially multiplexed fibers by the use of an OBR, is that one of the fibers presents a level of backscattering which is several dB larger than the other N-1 fibers. In this case the sum of N-1 backscattered powers can be considered like a background interference with respect to the high backscattering fiber. To fulfill this paradigm of operation, a special fiber, where the backscattering is strongly enhanced by the presence of MgO-based nanoparticles, has been used in this work. The fiber, whose cross-section SEM image is show in Fig. 1, has been designed to be an effective fiber amplifier working in the C-band (from 1530 to 1565 nm). For this reason, the core is co-doped by erbium and by a random distribution of MgO-based nanoparticles. In this contribution, the property of the fiber to be an amplifier is not exploited, since the exploited characteristic is the presence of nanoparticles and the relative backscattering generated by them. The fiber presents the typical size of a telecom fiber, with core diameter of roughly 10 μm and cladding diameter of 125 μm. This standard fiber size represents an advantage for the proposed operation since it makes the splicing procedure, with standard SMF-28 pigtails, quite trivial. It is worth noting that all the splices, created for the experimental section presented in this contribution, have been achieved by using an entry level fusion splicer (Fujikura 12-S), and by setting the SM to SM program. The obtained splice losses were acceptable in most of the cases.

The preform was fabricated by conventional MCVD (Modified Chemical Vapor Deposition) process, a flexible technique

mostly used for the production of specialty optical fibers based on silica [31]. We proposed a straightforward technique allowing to grow *in-situ* oxide nanoparticles in silica-based preforms due to high temperatures reached during the MCVD process [32]. The implemented principle is the spontaneous phase separation process: silicate systems can exhibit strong and stable immiscibility when they contain alkaline earth ions (MO, where M = Mg, Ca or Sr). For example, if a silicate glass containing few mol% MgO is heated, it will decompose into two phases: one silica-rich and one MgO-rich in shape of spherical particles. Thanks to this approach, no heat treatment is applied to the final fiber to form nanoparticles. The characteristics of the nanoparticles (size, size distribution) depends on the concentration of Mg.

To prepare the preform, a Ge-doped silica porous layer was deposited inside the silica substrate tube at a temperature of 1600 °C. The flow rates of $SiCl_4$, $GeCl_4$ and O_2 were 50, 37 and 750 cc/min, respectively. The porous core layer was immersed three times with 5 mL of the doping solution injected in the horizontally rotating tube. The composition of the ethanol-based doping solution is 0.1 mol/l of $MgCl_2$ and 10^{-4} mol/l of $ErCl_3$. The porous layer was dried at 1000 °C under an oxygen gas flow (2000 cc/min), then sintered by increasing the temperature up to 1860 °C. The tube was collapsed into the preform by heating above 2000 °C. The diameter of the preform was around 10 mm with a 0.8 mm core diameter. The optical fiber was drawn on a drawing tower by heating the preform at approximately 2000 °C. The external diameter of the fiber was 125 µm while the core diameter is about 10 µm.

The compositions of the optical preform and fiber were measured using Energy Dispersive X-ray (EDX) analyses. The average magnesium and germanium concentration vary along the length (axial direction) of the fiber. The highest magnesium and germanium concentrations are 1.7 and 0.4 at.%, respectively. The exact composition of the nanoparticles is unknown for this fiber, but it has been reported previously for other fibers that such nanoparticles are enriched with Mg [33].

Because of the presence of strong scattering in the core preform, given by the nanoparticles, the core appears white. This makes impossible to experimentally measure the core refractive index using a preform analyzer. Nevertheless, according to previous experience [32], and considering the concentration of the various dopants in the fiber core, it is possible to estimate the refractive index of the core substrate at a value varying from 1.7 to 4.0 $\times$ 10^{-3} higher with respect to the cladding index. It is also possible to estimate the average refractive index of the nanoparticles at 1.58. With those values, a random generated structure, statistically similar to the one shown in Fig. 1, has been simulated using a Finite Element Method (FEM) based software. Simulations have shown a multimode behavior, presumably given by the localization induced by the random pattern of nanoparticles [34]. The Mode Field Diameter (MDF) of the fundamental mode is reduced to 9.7 µm at 1550 nm, and the cut-off has moved to a wavelength larger than 2050 nm. These results are, clearly, variable since they depend on the fluctuation of the nanoparticle distribution, the fluctuation of their diameter, and the fluctuation of their refractive index. However, they give an understanding of the light propagation modification induced by the nanoparticles.

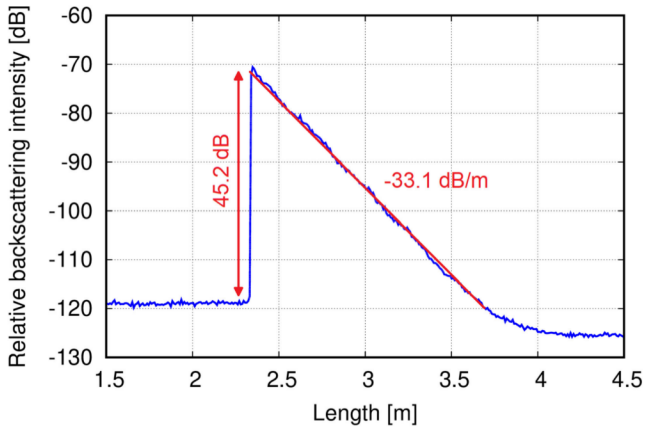

Fig. 2. Backscattered intensity along the fiber, i.e., the nanoparticles doped fiber spliced with the pigtail.

The backscattering properties of this fiber has been investigated by means of a commercial OBR (Luna Inc., OBR4600) [27]. A piece of NP fiber, 12 m long, has been spliced to a single mode pigtail fiber (SMF-28) terminating with a FC/APC connector. The pigtail fiber has been connected to the OBR. The first 2 m of the NP fiber have been maintained straight while the rest has been spooled in a 10 cm diameter spool. The OBR has been set to test the fiber with a spatial resolution of 0.1 mm. The internal laser operates by scanning from 1530 nm to 1572 nm. From Fourier analysis of the backscattered signal, it is possible to reconstruct the backscattered intensity along the length of the fiber, as it is shown in Fig. 2, where the relative intensity is mapped in log scale. Before the splice the level of backscattering given by the SMF pigtail is around -118 dB. Just after the splice the NP fiber shows a backscattering intensity which is around 45 dB higher. Then the backscattering decreases exponentially by 33 dB/m, till the minimum value, detectable by the OBR, is reached. A cut of 1.5 m of this fiber is, consequently, enough to extinguish the useful detectable scattering.

It is worth noting that the step of backscattering level created just after the splice between the SMF and the NP fiber can vary according to the quality of the splice and according to the local amount of backscattering. As the formation of MgO-based nanoparticles during the process of drawing is random, the backscattering presents a variance of few dB. This can be notice observing the blue curve slope which ripples around the fitting red slope. This fact also impacts on the value of the slope that can locally change by some decibels.

Another consideration to stress is related to the presence of erbium dopant inside the core glass compound. Since erbium is an active material, showing absorption and emission properties in the spectral region between 1530 nm to 1572 nm, it can contribute to the overall scattering of the fiber. However, this contribution is negligible as the backscattering signature of the fiber remains constant among different measurements in the same environment conditions, so that the backscattering

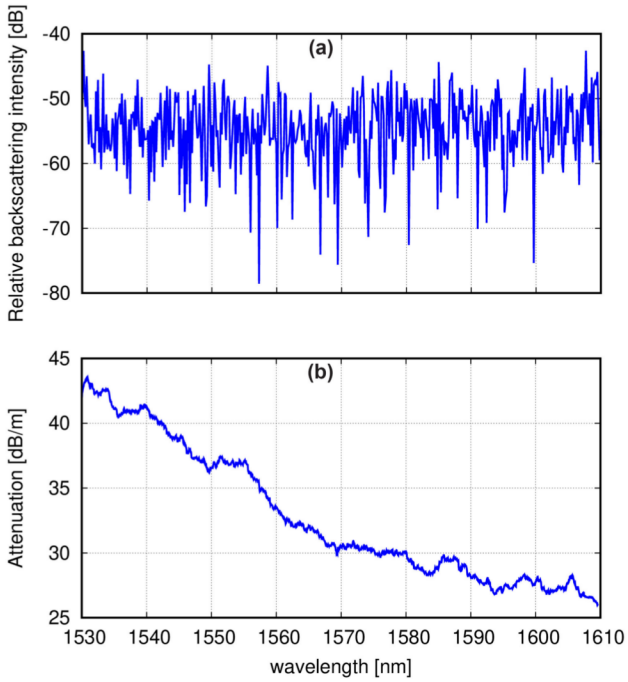

Fig. 3. Relative backscattering intensity over the spectral region of 1530–1610 nm, evaluated in the beginning of the NP fiber, at 2.5 meters distance from the OBR. (a) Spectral attenuation measured by the OBR after one meter of propagation.

realization can be correlated to the random geometrical distribution of the nanoparticles, which is deterministic [35].

Moreover, the concentration of erbium, used in this fiber, is 1.5×10^{24} ions/m^3, which is a moderate concentration. Since it is not possible to separate the absorption given by the erbium ions and the scattering induced by the nanoparticles, in order to have an estimation of the losses given by the erbium absorption, a standard telecom fiber, having a similar erbium concentration, has been tested with Luna OBR. The result shows an attenuation of 0.7 dB/m, which can be considered negligible with respect to the attenuation given by the nanoparticles.

Eventually, another aspect shall be considered. The scattering related losses are dominant and can be assimilated to a Rayleigh scattering of nanoparticles of higher refractive index surrounded by the silica core media with lower refractive index [33]. The high nanoparticle concentration, as well as the short distance between neighbor nanoparticles, suggests the effect of multiple scattering. To test this effect, a spectral measurement, using the Luna OBR, has been performed considering a 5 mm long cut of the fiber located at 2.5 m from the OBR. The backscattering spectrum has been scanned form 1530 nm to 1610 nm. As shown in Fig. 3(a), the chaotic spectrum is typical of disordered media, where multiple scattering is dominant. The properties of these material are exploited for demonstrating well-known effects such as random lasing [36], [37]. The spectral measurement has been taken in other positions of the NP fiber in order to investigate the variation of backscattering signal over the wavelength. Evaluating the backscattering signal drop, it has been possible to reconstruct the attenuation of the NP fiber in the range of 1530–1610 nm. The plot is shown in Fig. 3(b).

III. Working Principles

The possibilities offer by OBR system are strictly related to the capability of using a normal, inexpensive, SMF-28 fiber as a distributed sensor [25]. The length of the fiber and the resolution between two sensing points are limited by the amount of complex calculation that the OBR performs in order to reconstruct the backscattering spectra for each single sensing point. The fiber is, therefore, a 1D sensor that can become, when there is enough room in the area to sense, a 2D or 3D spatial sensor by properly bending and fitting it. However, a conspicuous number of applications, particularly in bio and medical fields, like mini-invasive medical devices, or devices for theragnostic applications, requires a distributed, real time, sensing taken from different location. In these applications the environment to test impedes to fit a single fiber sensor, possibly folded to follow the characteristic of the space to sense. [11], [14], [38]. In those cases, a solution consists in spatially multiplexing N fibers, feeding the OBR by the help of a switch. However, each fiber shall be interrogated in different time slots, driving to a time domain multiplexing [26]. The drawback of this method is the drastic reduction (by a factor much larger than N) of the interrogation frequency, which is already limited by the capability of the OBR. A spatial multiplexing obtained by a simultaneous interrogation of all the multiplexed fibers can avoid the reduction of the sensing frequency.

The idea developed in this work is based on the previously described NP fiber, where the backscattering level is several dB larger than a SM fiber, but enough low to permit the application of OFDR basic principles [24], [25]. The use of other kinds of enhanced backscattering fiber for OBR operation has been already exploited by Yan *et al.* for real time monitoring of solid oxide fuel cell [39]. However, the use of NP fiber for spatial multiplexing between parallel sensors has not yet been explored. The proposed NP fiber shows better performances, in terms of uniformity of backscattering enhancement and attenuation, with respect to the one used in [39]. Furthermore, from the technological point of view, in terms of cost/effectiveness, the proposed NP fiber is more efficient. After the fabrication of the preform, it is possible to draw hundreds of meters of fiber at a relatively low cost and time (using the same drawing process as the one for a standard SMF28).

The multiplexing implementation is based on the capability of placing cuts of NP fiber in an optical circuit composed by a parallel of fibers where the NP fiber spatially overlaps the other SM fibers. The schematic is shown in Fig. 4. The spatial multiplexed sensors are obtained by a parallel of optical fibers, connected by a coupler $1\times$N. Every fiber line is composed by a fiber separator L_i, obtained using a standard SMF-28, and a cut of nanoparticles doped fiber S_i spliced at the end.

To formalize this scheme, it is necessary to make some simple assumptions:

- every multiplexed channel is to be considered identical because it is built only with two kinds of fiber (SMF-28 and NP fiber);
- the loss of SMF is negligible for the short length taken in consideration;

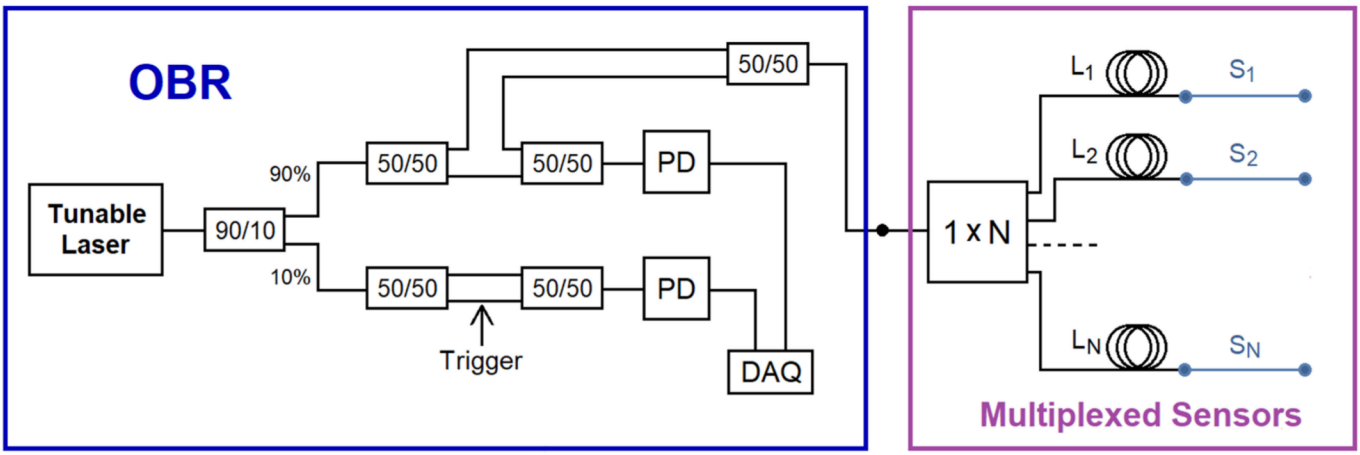

Fig. 4. Schematic of fiber multiplexing using nanoparticles doped fibers. The blue rectangle represents the OBR internal schematic, while the purple square represents the N multiplexed sensors connected in parallel using a 1 × N coupler. Fiber separators L_i, with different length, are used to permit the fiber multiplexing.

- the NP fiber, used for sensing, presents a constant attenuation;
- Extra losses given by the coupler and by the splices are not considered.
- The backscattering generated by the involved fibers (SMF-28 and NP fiber) is treated as a deterministic signal.

With these hypotheses the backscattering power detected in the position z, by the OBR, on the i^{th} channel is:

$$P_{s,i}(z) = \begin{cases} P_{SMF} & 0 \le z \le L_i \\ P_{SMF} \cdot G \cdot e^{-2\alpha z} & L_i \le z \le (L_i + S_i) \end{cases} \quad (1)$$

Where P_{SMF} is the backscattering power of a standard SMF-28 telecom fiber, G represents the backscattering gain of the NP fiber with respect to the SMF-28 and α is the NP fiber attenuation. The factor 2 at the exponent represents the forth and back path of the light that returns to the OBR. Clearly, the second equation is applied to the NP fiber cut at the termination, while the first equation is applied to the SMF pigtail.

The total power detected by the OBR is written as:

$$P_d(z) = \sum_{i=1}^{N} P_{s,i}(z) + \sum_{i=1}^{N} \sum_{j>i}^{N} K_{ij} \sqrt{P_{s,i}(z) P_{s,j}(z)} \quad (2)$$

The first term of this equation takes in consideration the contribution of backscattering given by every line in the parallel setup, while the second term takes in consideration the interference of the backscattered signal at a certain position z. However, the second term shall be neglected as it is characterized by an expected value equal to zero and a negligible standard deviation, that has the same level of the background noise of the Luna photodiode. So, at the net of all contributions, the average weight of all the interference components results to be null. The reason for this is given by the multiple scattering behaviour of the Rayleigh scattering. Like the NP fiber, the standard SMF-28 fiber presents, at a certain position z, a similar chaotic backscattering spectrum. Every frequency component presents its own random phase, uniformly distributed between 0 and 2π. It is easy to demonstrate that the summation of every interference contribution over the entire spectrum has an expected value equal to zero, and the overall standard deviation of the interference contribution is negligible, so that eq. (2) becomes:

$$P_d(z) = \sum_{i=1}^{N} P_{s,i}(z) \quad (3)$$

All the experiments performed by use of the proposed multiplexed method, have shown that the total backscattered power is the sum of the power of each single line, with negligible contribution given by the interference terms.

In order to obtain an effective multiplexing, it is necessary that the backscattering generated in the NP fiber region is much greater than the one generated the SMF-28. Furthermore, considering the fibers parallel, the NP fiber must overlap only pigtails located in the other lines and not the other NP fibers. To implement this behaviour, the pigtails length L_i must be carefully chosen as:

$$L_N > (L_{N-1} + S_{N-1}) > \ldots > (L_1 + S_1) \quad (4)$$

The worst case is represented by the first portion of NP fiber which overlaps *N-1* SMF pigtails. Considering this disadvantaged case, it is possible to define the signal-to-background interference ratio *SBR* as:

$$SBR = \frac{P_{sensor}}{P_{background}} = \frac{P_{SMF} \cdot G \cdot e^{-2\alpha z}}{(N-1) \cdot P_{SMF}} = \frac{G e^{-2\alpha z}}{N-1} \quad (5)$$

It is also possible to define a target signal-to-background interference ratio, SBR_T, as the maximum tolerable level of interference generated by the *N-1* pigtails over the NP fiber sensor:

$$SBR_T \le \frac{G e^{-2\alpha z}}{N-1} \quad (6)$$

By means of simple mathematical passages, it is possible to invert the equation and to obtain the maximum length of NP fiber z_{max}, which permits to fulfil the condition of acceptable interference generated by the other SMF pigtails:

$$z_{max} = \frac{1}{2\alpha} \ln\left[\frac{G}{(N-1) \cdot SBR_T}\right] \quad (7)$$

To serve as an example, it is possible to consider a situation with 8 multiplexed sensors and the following parameters:

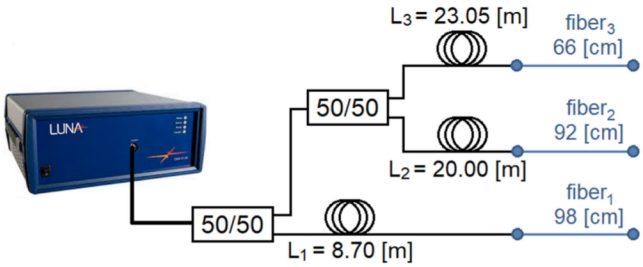

Fig. 5. Experimental setup used to demonstrate the paradigm of spatial multiplexing of fiber sensors. The core working principle is the use of high scattering nanoparticles doped fibers.

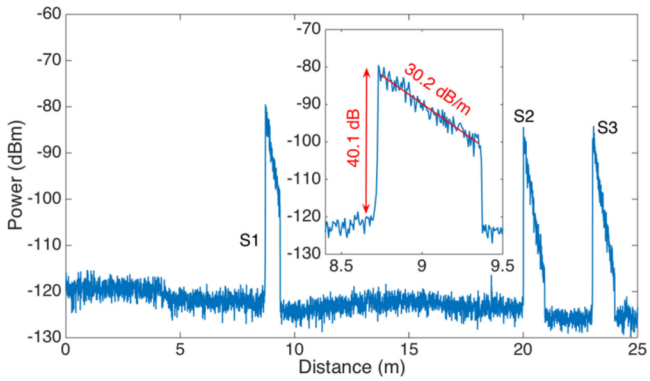

Fig. 6. Backscattering output power of the experimental setup registered by the OBR.

$G_{dB} = 40$ dB, $SBR_{T,dB} = 20$ dB, $\alpha_{dB} = 10$ dB. The maximum cut of NP fiber results to be $z_{max} = 57.7$ cm. In general, the applications for this kind of multiplexed sensing do not required a long cut of NP fiber: 10 cm of sensing fiber can be more than enough. For such a length the system can be properly scaled to accommodate 50 multiplexed fiber sensors. Furthermore, the manufacturing of NP fiber is promising in terms of optimization of maximum scattering gain over the attenuation.

IV. Experimental Setup and Results

As a proof of concept of the proposed multiplexing method an experimental setup, having three cuts of NP fiber, has been prepared. The target of the experiments is to sense temperature and strain by placing the NP sensing fibers in the proper location.

The basic multiplexing setup is shown in Fig. 5. Three fiber channels are connected by the help of two 1×2 couplers. The first fiber sensors ($fiber_1$) is 98 cm long and it is spliced to a separator pigtail of 8.70 m; the second fiber sensor ($fiber_2$) is 92 cm long and its pigtail is 20 m long; the third fiber sensor ($fiber_3$) is 66 cm long and its pigtail is 23.05 m long. It is worth noting that the length L_i of the separator takes in consideration the couplers pigtails length and a properly SMF portion. This basic setup has been investigated connecting the output branch of the first coupler to the OBR. The backscattering power distribution is shown in Fig. 6. The OBR can distinguish the backscattering traces produced by the NP fibers fragments with respect to the low level of backscattering exhibited by the SMF.

The backscattering peak exhibited by the shortest line, i.e., fiber1, is roughly 3 dB higher with respect to fiber2 and fiber3,

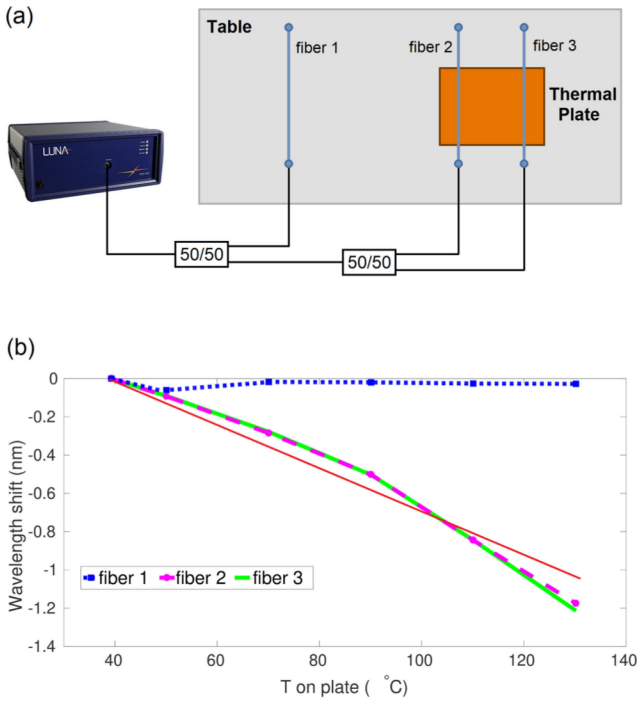

Fig. 7. Schematic of the setup for temperature measurement (a); wavelength shift obtained by varying the temperature of the thermal plate (b).

this is because it passes only through one coupler, so that the scan laser, sent by the OBR, is not divided anymore. As stressed in the previous section, it is important to notice that the level of backscattering gain after the splice, as well as the decay of backscattering, is dependent, in part, on the local MgO-based nanoparticles concentration and on the quality of the splice. For example, the first cut of NP fiber presents a gain of 40.1 dB and a backscattering attenuation of 30.2 dB/m, slightly different for the results shown in Fig. 2. Using the proposed basic setup, measurements of temperature and strain have been taken.

A. Temperature Measurements

For temperature measurement, the setup has been arranged by laying down two fibers, precisely $fiber_2$ and $fiber_3$, on a thermal plate, while $fiber_1$ is maintained on the laboratory table sensing the environment temperature. The temperature of the thermal plate has been increased by 40 °C to 130 °C. The temperature has been checked by means of a thermocouple, located in proximity of the NP fiber sensors. The schematic of the setup is shown in Fig. 7(a).

The temperature has been measured by setting the OBR to detect the spectral shift of the backscattering spectra in predefined points, roughly 30 cm after each splice, for all the three NP fiber cuts. While the temperature reference, to calculate the wavelength shift of $fiber_2$ and $fiber_3$ has been set to 40 °C, the temperature reference of $fiber_1$ has been considered to be the temperature of the laboratory (26 °C). From Fig. 7(b), it is possible to see that $fiber_1$ has detected a nearly constant temperature as the wavelength shift is roughly zero. The small detected ripple has been given by the body temperature of the operator, who

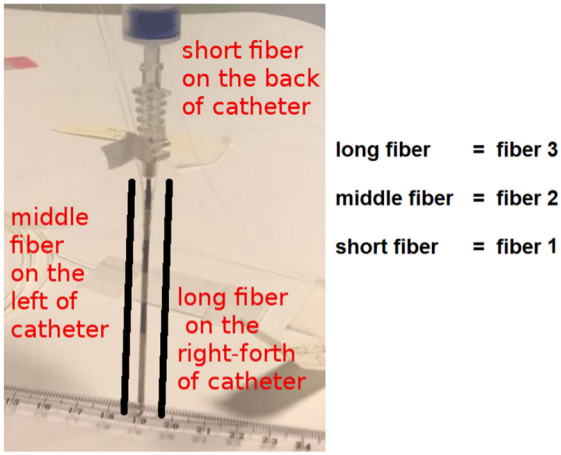

Fig. 8. NP fiber sensors location on the epidural needle. According to the picture the short fiber is on the back, the middle fiber is on the left and the long fiber is on the right.

moved the fiber on the lab table during the first measurements. Simultaneously, $fiber_2$ and $fiber_3$ have measured the temperature increase on the thermal plate. The curves of $fiber_2$ and $fiber_3$ are not perfectly linear, mainly because the mismatch of the temperature measured by the fibers and by the thermocouple. In fact, the tip of the reference thermocouple is significantly big with respect to the NP fibers so that the reference temperature is more dependent on the environment temperature, while the temperature measured by the fibers is closer to the real temperature of the thermal plate.

Although this mismatch, the red fitting curve, depicted in Fig. 7(b), shows a slope of roughly 11.2 pm/°C, very similar to the sensitivity of a SMF-28. More accurate measurements, obtained by submerging the NP fiber and a reference SMF in a controlled temperature water bath, show that the sensitivity of the NP fiber is, basically, the same as a standard SMF-28 [35].

B. Strain Measurements

In order to test the spatial distributed sensing multiplexing to measure the strain, a particular setup has been prepared. The three NP fiber sensors has been fixed, by means of an epoxy glue, to a Tuohy needle for epidural anesthesia: ZZOR18G model, 8 cm length, 18 Gauge thickness equivalent to 1.32 mm of outer diameter and 1.09 mm of inner diameter, (Balton, Poland), with the same method used in [38]. In particular, the last 4-5 cm of the NP fibers have been carefully fixed longitudinally on the needle, arranged in a shape forming an angle of 120° with respect to each other. The schematic of the NP fiber sensors is depicted in Fig. 8. According to the orientation of Fig. 8, the short fiber ($fiber_1$) is positioned in the back part of the needle, while $fiber_2$ and $fiber_3$ are on the front/lateral side.

The strain has been imposed by pressing the needle on the laboratory table to obtain a convex bending, in the direction of the short fiber. Three qualitative amounts of pressure have been taken in consideration, to obtain: a weak bending, a medium bending and a strong bending.

It is worth noting that the choice of qualitative strain sensing is driven by the need to show the capability to obtain the

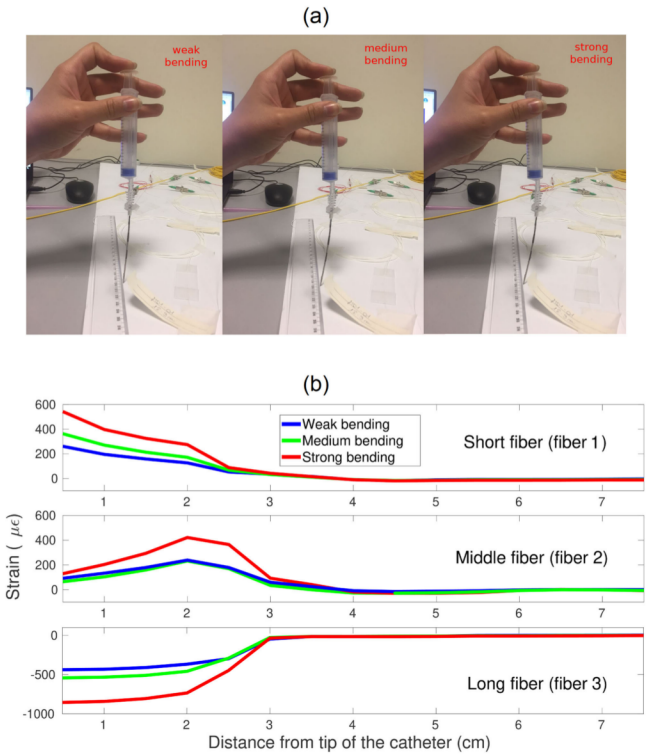

Fig. 9. Three different level: weak, medium and strong, of convex bending of the epidural needle toward the direction of short fiber. (a) Measured strain of each fiber by means of OBR.

simultaneous distributed multiplexing, thus proving the effectiveness of the paradigm based on high backscattering NP fiber sensors. Calibrations and precise strain measurements are not the target of this work.

The qualitative amount of bending is depicted in Fig. 9(a), while the measured strain of each fiber is shown in Fig. 9(b). The OBR is capable to detect the spectral shift occurring in the condition of strain correlated to the reference value of straight needle, which is equivalent to a condition with no strain applied. The conversion between spectral shift and strain has been calculated assuming that the NP fiber has the same physical and mechanical characteristics, including the strain coefficient, of a standard SMF-28. This similarity has been discussed in [35].

From Fig. 9(b) it is possible to see that the strain of $fiber_1$ is positive and growing with the increase of bending, since $fiber_1$ is stretched following the convexity of the bending. The middle fiber ($fiber_2$) shows a sort of torsion which becomes more evident when the needle is strongly bent, while $fiber_3$ follows the concavity of the bending in opposition to $fiber_2$ and $fiber_1$ showing an increasing negative strain. These results, even if qualitative, are in good agreement with the expectations. They permit to validate the use of the simultaneous multiplexed setup, showing the capability of the special NP fiber to effectively detect the strain and its sign.

A second experience has been performed by inverting the convexity of the bending, as shown in Fig. 10(a). The bending direction is, again, toward the direction identified by $fiber_1$. However, in this case, the bending presents a concave shape. Strain results are shown in Fig. 10(b). In this case the $fiber_1$

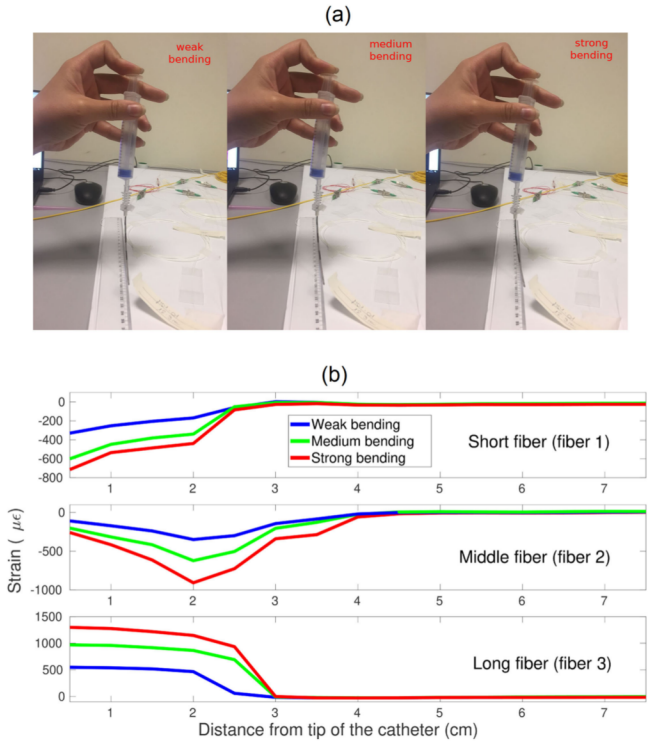

Fig. 10. Three different level: weak, medium and strong, of concave bending of the epidural needle toward the direction of short fiber. (a) Measured strain of each fiber by means of OBR.

presents an evolution very similar to the first inset of Fig. 9(b), with a quite similar trend of strain increase. The only difference is that the strain has negative sign, since $fiber_1$ has been bent in concave shape. Regarding $fiber_2$ and $fiber_3$, also in this case the needle presents a sort of torsion that forces $fiber_2$ to have a maximum of negative strain at 2 cm form the needle tip, and push $fiber_3$ to follow a convex bending. Both $fiber_2$ and $fiber_3$ present a strain dynamic very similar to that shows in Fig. 9(b), where the difference is found in the sign of the strain which is inverted.

V. Conclusion

In this work a novel paradigm for implementing a simultaneous distributed sensing multiplexing by means of multiple fiber sensors connected in a parallel optical circuit through a 1×N coupler is presented, theoretically investigated, and experimentally proved. The core working principle is based on the use of a special MgO-based nanoparticles doped fiber, which presents a level of backscattering that is several dB (40 or more) larger with respect to a SMF-28, the standard fiber used in telecommunications. Because this high scattering, it is possible to create an optical fiber parallel where the NP fiber overlap SM pigtails, so that the combined backscattering can feed an OFDR-based detection system (like an OBR). Since the NP fiber backscattering overwhelms the backscattering coming from the other lines of the circuit, the OBR can resolve the backscattering detection. The back scattering coming from the other lines acts like a negligible background interference, which shall be maintained under a certain level. With a simple model it is possible to design all the parameter of this new multiplexing paradigm to fulfill the required level of tolerable background interference and to find the correct length of the NP fiber.

The real advantage of this new paradigm over the proposed multiplexing strategy shown in literature, is that, in this case, the multiplexing is obtained simultaneously and not implementing a time division multiplexing interrogation by the use of an optical switch. Such a simultaneous interrogation avoids any kind or reduction of the interrogation frequency.

This solution is also easy to implement, since the NP fiber presents the same size of a SMF-28, and it is easily sliceable. Furthermore, this fiber has similar characteristic of sensitivity to temperature and strain with respect to a SMF-28. Experimental results have shown the feasibility of this idea. Measurements of temperature and strain have been taken with a simultaneous distributed multiplexing setup. Results are in good agreements with the expectations, demonstrating both the sensing accuracy of the NP fiber and the possibility to arrange a N-fiber multiplexed system.

This new method of multiplexing is particularly important for biomedical applications, allowing both distributed sensing and spatial multiplexing over multiple fibers. The possibility to arrange arbitrarily the geometry of each sensing fiber, for example around the inner wall of a catheter or in 3-dimensional geometries during thermo-therapies opens unprecedented scenarios, considering that each sensor operates as a distributed detection with gage length close to 1 mm. In comparison to spatial division multiplexing techniques that operate with multi-core fibers, here the sensors are not located in the same fiber but can be placed in any location.

Acknowledgment

The authors would like to thank S. Trzesien and M. Ude (INPHYNI, Nice, France) for the fabrication of the fiber.

References

[1] E. Udd and W. B. Spillman, Jr., *Fiber Optic Sensors: An Introduction for Engineers and Scientists*. Hoboken, NJ, USA: Wiley, Oct. 11, 2011.
[2] B. Lee, "Review of the present status of optical fiber sensors," *Opt. Fiber Technol.*, vol. 9, no. 2, pp. 57–79, Apr. 1, 2003.
[3] Biological Evaluation of Medical Devices, ISO 10993, Int. Org. Standardization: Geneva, Switzerland, 1995.
[4] E. Schena, D. Tosi, P. Saccomandi, E. Lewis, and T. Kim, "Fiber optic sensors for temperature monitoring during thermal treatments: An overview," *Sensors*, vol. 16, no. 7, Jul. 22, 2016, Art. no. 1144.
[5] S. J. Mihailov, "Fiber Bragg grating sensors for harsh environments," *Sensors*, vol. 12, no. 2, pp. 1898–1918, Feb. 10, 2012.
[6] Y. J. Rao, "Recent progress in applications of in-fibre Bragg grating sensors," *Opt. Lasers Eng.*, vol. 31, no. 4, pp. 297–324, Apr. 1, 1999.
[7] A. D. Kersey, T. A. Berkoff, and W. W. Morey, "Multiplexed fiber bragg grating strain-sensor system with a fiber Fabry–Perot wavelength filter," *Opt. Lett.*, vol. 18, no. 16, pp. 1370–1372, Aug. 15, 1993.
[8] J. W. Arkwright *et al.*, "In-vivo demonstration of a high resolution optical fiber manometry catheter for diagnosis of gastrointestinal motility disorders," *Opt. Express*, vol. 17, no. 6, pp. 4500–4508, Mar. 16, 2009.
[9] J. W. Arkwright *et al.*, "Design of a high-sensor count fibre optic manometry catheter for in-vivo colonic diagnostics," *Opt. Express*, vol. 17, no. 25, pp. 22423–31, Dec. 7, 2009.
[10] H. Liu *et al.*, "Shape tracking of a dexterous continuum manipulator utilizing two large deflection shape sensors," *IEEE Sensors J.*, vol. 15, no. 10, pp. 5494–5503, Oct. 1, 2015.

[11] X. He, J. Handa, P. Gehlbach, R. Taylor, and I. Iordachita, "A submillimetric 3-DOF force sensing instrument with integrated fiber Bragg grating for retinal microsurgery," *IEEE Trans. Biomed. Eng.*, vol. 61, no. 2, pp. 522–534, Feb. 2014.
[12] D. Feng, W. Zhou, X. Qiao, and J. Albert, "Compact optical fiber 3D shape sensor based on a pair of orthogonal tilted fiber Bragg gratings," *Sci. Rep.*, vol. 5, Nov. 30, 2015, Art. no. 17415.
[13] D. Tosi, E. Schena, C. Molardi, and S. Korganbayev, "Fiber optic sensors for sub-centimeter spatially resolved measurements: Review and biomedical applications," *Opt. Fiber Technol.*, vol. 43, pp. 6–19, Jul. 31, 2018.
[14] M. Jelbuldina, A. V. Korobeinyk, S. Korganbayev, V. J. Inglezakis, and D. Tosi, "Fiber Bragg grating based temperature profiling in ferromagnetic nanoparticles-enhanced radiofrequency ablation," *Opt. Fiber Technol.*, vol. 43, pp. 145–152, Jul. 31, 2018.
[15] X. Liu, I. I. Iordachita, X. He, R. H. Taylor, and J. U. Kang, "Miniature fiber-optic force sensor based on low-coherence Fabry-Pérot interferometry for vitreoretinal microsurgery," *Biomed. Opt. Express*, vol. 3, no. 5, pp. 1062–1076, May 1, 2012.
[16] J. W. Arkwright *et al.*, "Measurement of muscular activity associated with peristalsis in the human gut using fiber Bragg grating arrays," *IEEE Sensors J.*, vol. 12, no. 1, pp. 113–117, Jan. 2012.
[17] E. Aranda-Michel *et al.*, "Miniaturized robotic end-effector with piezoelectric actuation and fiber optic sensing for minimally invasive cardiac procedures," *IEEE Sensors J.*, vol. 18, no. 12, pp. 4961–4968, Jun. 15, 2018.
[18] A. D. Kersey *et al.*, "Fiber grating sensors," *J. Lightw. Technol.*, vol. 15, no. 8, pp. 1442–1463, Aug. 1997.
[19] F. Zhang *et al.*, "Dynamic fiber Bragg grating sensor array with increased wavelength-division multiplexing density and low crosstalk," *Opt. Eng.*, vol. 56, no. 3, Mar. 2017, Art. no. 037101.
[20] E. Lindner *et al.*, "Trends and future of fiber Bragg grating sensing technologies: Tailored draw tower gratings (DTGs)," in *Proc. SPIE Photon. Europe*, Brussels, Belgium, May 2014, vol. 9141, Art. no. 91410X.
[21] T. Mizuno, H. Takara, A. Sano, and Y. Miyamoto, "Dense space-division multiplexed transmission systems using multi-core and multi-mode fiber," *J. Lightw. Technol.*, vol. 34, no. 2, pp. 582–592, Jan. 15, 2016.
[22] I. Gasulla, D. Barrera, J. Hervás, and S. Sales, "Spatial division multiplexed microwave signal processing by selective grating inscription in homogeneous multicore fibers," *Sci. Rep.*, vol. 7, Jan. 30, 2017, Art. no. 41727.
[23] J. Hervás *et al.*, "Microwave photonics for optical sensors," *IEEE J. Sel. Topics Quantum Electron.*, vol. 23, no. 2, pp. 327–339, Mar. 2017.
[24] X. Bao and L. Chen, "Recent progress in distributed fiber optic sensors," *Sensors*, vol. 12, no. 7, pp. 8601–8639, Jun. 26, 2012.
[25] M. Froggatt and J. Moore, "High-spatial-resolution distributed strain measurement in optical fiber with Rayleigh scatter," *Appl. Opt.*, vol. 37, no. 10, pp. 1735–1740, Apr. 1, 1998.
[26] B. J. Soller, D. K. Gifford, M. S. Wolfe, and M. E. Froggatt, "High resolution optical frequency domain reflectometry for characterization of components and assemblies," *Opt. Express*, vol. 24, no. 13, pp. 666–674, Jan. 24, 2005.
[27] Luna technologies, OBR 4600. [Online]. Available: http://lunainc.com/product/sensing-solutions/obr-4600/
[28] D. Farnesi *et al.*, "Quasi-distributed and wavelength selective addressing of optical micro-resonators based on long period fiber gratings," *Opt. Express*, vol. 23, no. 16, pp. 21175–21180, Aug. 10, 2015.
[29] P. Saccomandi, E. Schena, and S. Silvestri, "Techniques for temperature monitoring during laser-induced thermotherapy: An overview," *Int. J. Hyperthermia*, vol. 29, no. 7, pp. 609–619, Nov. 1, 2013.
[30] F. Parent *et al.*, "Enhancement of accuracy in shape sensing of surgical needles using optical frequency domain reflectometry in optical fibers," *Biomed. Opt. Express*, vol. 8, no. 4, pp. 2210–2221, Apr. 1, 2017.
[31] J. B. Mac Chesney, P. B. Oapos Connor, and H. M. Presby, "A new technique for the preparation of low-loss and graded-index optical fibers," *Proc. IEEE*, vol. 62, no. 9, pp. 1280–1281, Sep. 1974.
[32] W. Blanc *et al.*, "Fabrication of rare earth-doped transparent glass ceramic optical fibers by modified chemical vapor deposition," *J. Amer. Ceram. Soc.*, vol. 94, no. 8, pp. 2315–2318, 2011.
[33] W. Blanc, C. Guillermier, and B. Dussardier, "Composition of nanoparticles in optical fibers by secondary ion mass spectrometry," *Opt. Mater. Express*, vol. 2, no. 11, pp. 1504–1510, 2012.
[34] M. Segev, Y. Silberberg, and D. N. Christodoulides, "Anderson localization of light," *Nat. Photon.*, vol. 7, pp. 197–204, 2013.
[35] C. Molardi, S. Korganbayev, W. Blanc, and D. Tosi, "Characterization of a nanoparticles-doped optical fiber by the use of optical backscatter reflectometry," in *Proc. SPIE/COS Photonics Asia*, Beijing, China, vol. 10821, Oct. 2018, Art. no. 1082121.
[36] D. S. Wiersma, "The physics and applications of random lasers," *Nat. Phys.*, vol. 4, pp. 359–367, 2008.
[37] B. Abaie, E. Mobini, S. Karbasi, T. Hawkins, J. Ballato, and A. Mafi, "Random lasing in an Anderson localizing optical fiber," *Light Sci. Appl.*, vol. 6, 2017, Art. no. e17041.
[38] A. Beisenova, A. Issatayeva, D. Tosi and C. Molardi, "Fiber-optic distributed strain sensing needle for real-time guidance in epidural anesthesia," *IEEE Sensors J.*, vol. 18, no. 19, pp. 8034–8044, Oct. 1, 2018.
[39] A. Yan *et al.*, "Distributed optical fiber sensors with ultrafast laser enhanced rayleigh backscattering profiles for real-time monitoring of solid oxide fuel cell operations," *Sci. Rep.*, vol. 7, no. 1, pp. 9360–9369, 2017.